

## Carboxylate as the Protonation Site in (Peroxo)diiron(III) Model Complexes of Soluble Methane Monooxygenase and Related Diiron Proteins

Loi H. Do,<sup>†</sup> Takahiro Hayashi,<sup>‡</sup> Pierre Moënne-Loccoz,<sup>\*,‡</sup> and Stephen J. Lippard<sup>\*,†</sup>

Department of Chemistry, Massachusetts Institute of Technology, Cambridge, Massachusetts 02139, and Department of Science and Engineering, School of Medicine, Oregon Health and Science University, Beaverton, Oregon 97006

Received November 27, 2009; E-mail: plocco@ebs.ogi.edu; lippard@mit.edu

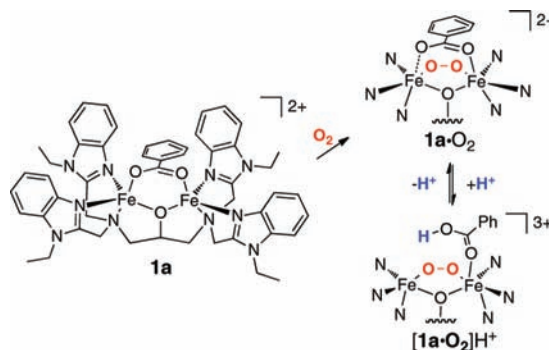
Dioxygen activation by carboxylate-bridged diiron enzymes is involved in essential biological processes ranging from DNA synthesis and hydrocarbon metabolism to cell proliferation.<sup>1–3</sup> The carboxylate-bridged diiron superfamily of proteins includes ribonucleotide reductase (RNR),<sup>4</sup>  $\Delta^9$  desaturase,<sup>5</sup> bacterial multicomponent monooxygenases (BMMs),<sup>6,7</sup> and most recently human deoxyhypusine hydroxylase (hDOHH).<sup>3</sup> In all of these systems, the O<sub>2</sub> reduction step proceeds through a (peroxo)-diiron(III) intermediate in which the resulting peroxo ligand is proposed to bridge two iron atoms in a  $\mu$ -1,2 or  $\mu$ - $\eta^2\eta^2$  coordination mode.<sup>8–10</sup> Extensive studies of soluble methane monooxygenase (sMMO), a BMM family member that oxidizes methane to methanol, reveal that the generation and activation of Fe<sub>2</sub>O<sub>2</sub> units requires protons.<sup>11,12</sup> Given the complexity of protein environments, identifying the sites involved in such proton translocation processes and their effect on O<sub>2</sub> activation is not a trivial undertaking.

To shed light on the possible role of protons in the dioxygen activation chemistry at carboxylate-bridged diiron enzyme active sites, we investigated the reaction of H<sup>+</sup> with a well-characterized synthetic ( $\mu$ -peroxo)( $\mu$ -carboxylato)diiron(III) complex, [Fe<sub>2</sub>( $\mu$ -O<sub>2</sub>)(*N*-EtHPTB)( $\mu$ -PhCO<sub>2</sub>)]<sup>2+</sup> (**1a**·O<sub>2</sub>).<sup>13,14</sup> The dinucleating *N*-EtHPTB ligand provides kinetic stabilization of the Fe<sub>2</sub>O<sub>2</sub> core, and the benzoate group serves as a good mimic of the Asp and Glu carboxylate side chains in the protein diiron centers. By application of several spectroscopic methods, we show that the reaction of H<sup>+</sup> with **1a**·O<sub>2</sub> results in protonation at the carboxylate unit rather than the peroxo ligand (Scheme 1). This work provides experimental support for recent theoretical studies suggesting that (hydroperoxo)diiron(III) species of nonheme diiron enzymes are too reactive to be isolable protein intermediates.<sup>15</sup>

To aid spectral interpretation of results obtained during studies of the parent [Fe<sub>2</sub>(*N*-EtHPTB)( $\mu$ -PhCO<sub>2</sub>)]<sup>2+</sup> complex (**1a**), two related diiron(II) precursors were synthesized (Supporting Information). One is [Fe<sub>2</sub>(*N*-EtHPTB)(Ph<sup>13</sup>CO<sub>2</sub>)]<sup>2+</sup> (**1b**), which contains a <sup>13</sup>C-enriched carboxylate ligand, and the other is [Fe<sub>2</sub>(*N*-EtHPTB)(C<sub>6</sub>F<sub>5</sub>CO<sub>2</sub>)]<sup>2+</sup> (**2**), in which the benzoate ring is fluorinated.

Exposure of **1a** to O<sub>2</sub> in CH<sub>3</sub>CN at –30 °C generates a deep blue-green solution (**1a**·O<sub>2</sub>) with  $\lambda_{\text{max}}$  at 590 nm.<sup>13</sup> Addition of an acetonitrile solution of [H(OEt<sub>2</sub>)<sub>2</sub>][(3,5-(CF<sub>3</sub>)<sub>2</sub>C<sub>6</sub>H<sub>3</sub>)<sub>4</sub>B] (H[Bar<sup>F</sup><sub>4</sub>]) to **1a**·O<sub>2</sub> red-shifts the peroxo-to-iron(III) charge transfer band to ~600 nm (Figure 1). This absorption is assigned

Scheme 1. Reaction of Dioxygen with **1a** and H<sup>+</sup> <sup>a</sup>



<sup>a</sup> A possible structure for [1a·O<sub>2</sub>]H<sup>+</sup> is depicted; the five-coordinate iron may be further coordinated by solvent in solution, and the bound benzoic acid might be hydrogen-bonded to the peroxo ligand.

to the formation of a new [1a·O<sub>2</sub>]H<sup>+</sup> species that maximizes with addition of ~1.5 equiv of H[Bar<sup>F</sup><sub>4</sub>]. The spectrum of **1a**·O<sub>2</sub> is restored upon addition of 2.0 equiv of NEt<sub>3</sub> (Figure 1, inset), indicating that protonation does not lead to irreversible decomposition of the **1a**·O<sub>2</sub> unit. Reaction of **2** with O<sub>2</sub> affords [Fe<sub>2</sub>( $\mu$ -O<sub>2</sub>)(*N*-EtHPTB)( $\mu$ -C<sub>6</sub>F<sub>5</sub>CO<sub>2</sub>)]<sup>2+</sup> (**2**·O<sub>2</sub>), which exhibits a broad absorption feature centered at ~600 nm. When H[Bar<sup>F</sup><sub>4</sub>] is titrated into a solution of **2**·O<sub>2</sub>, a small bathochromic shift to ~610 nm occurs (Figure S1). Unlike **1a**·O<sub>2</sub>, **2**·O<sub>2</sub> requires ~3.0 equiv of H[Bar<sup>F</sup><sub>4</sub>] to fully generate the protonated species [2·O<sub>2</sub>]H<sup>+</sup>. Given that pentafluorobenzoate, for which the acid

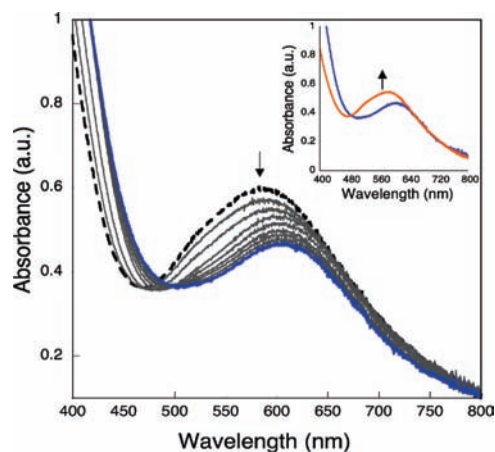


Figure 1. UV–vis absorption spectra of **1a**·O<sub>2</sub> (112  $\mu$ M in CH<sub>3</sub>CN, –30 °C) before (dotted trace) and after (blue trace) addition of 2.0 equiv of H[Bar<sup>F</sup><sub>4</sub>]. Inset: restoration of the initial spectrum (orange trace) upon treatment with 2.0 equiv of NEt<sub>3</sub>.

<sup>†</sup> Massachusetts Institute of Technology.

<sup>‡</sup> Oregon Health and Science University.

has a  $pK_a$  of 1.2, is more electron deficient than benzoate (acid  $pK_a = 4.6$ ), the greater amount of  $H^+$  necessary to produce  $[2 \cdot O_2]H^+$  from  $2 \cdot O_2$  compared to  $[1a \cdot O_2]H^+$  from  $1a \cdot O_2$  suggests either that the carboxylate ligand influences the basicity of the protonation site or that it is itself the proton acceptor.

To determine whether a (hydroperoxo)diiron(III) species may form upon addition of  $H^+$  to  $1a \cdot O_2$  or  $2 \cdot O_2$ ,  $^{57}Fe$  Mössbauer and resonance Raman (RR) spectra were recorded to examine possible changes in the  $Fe_2O_2$  core. In the absence of  $H^+$ , the Mössbauer spectrum of a frozen solution of  $1a \cdot O_2$  in  $CH_3CN$  can be fit to a single iron site, with  $\delta = 0.53(2)$  mm/s and  $\Delta E_Q = 0.71(2)$  mm/s (Figure S2A). Addition of  $H[Bar^F_4]$  to  $1a \cdot O_2$  gives  $[1a \cdot O_2]H^+$  having the same isomer shift ( $\delta = 0.53(2)$  mm/s) and a slightly larger quadrupole splitting parameter ( $\Delta E_Q = 0.80(2)$  mm/s) (Figure S2B). For comparison, the Mössbauer spectra of  $2 \cdot O_2$  and  $[2 \cdot O_2]H^+$  were also recorded. The (peroxo)diiron(III) complex of **2** has  $\delta = 0.53(2)$  mm/s and  $\Delta E_Q = 0.77(2)$  mm/s (Figure S2C), whereas the protonated  $[2 \cdot O_2]H^+$  form exhibits parameters of  $\delta = 0.54(2)$  mm/s and  $\Delta E_Q = 0.84(2)$  mm/s (Figure S2D). The similar isomer shifts obtained for  $1a \cdot O_2$ ,  $[1a \cdot O_2]H^+$ ,  $2 \cdot O_2$ , and  $[2 \cdot O_2]H^+$  are indicative of iron(III) centers, and the small increase in  $\Delta E_Q$  values for the protonated forms implies that only minor changes occur in the coordination environment.

To investigate more directly the nature of the peroxo moiety,  $Fe-O$  and  $O-O$  vibrations were measured by RR spectroscopy for species generated with both  $^{16}O_2$  and  $^{18}O_2$ . As previously reported,<sup>13</sup>  $1a \cdot O_2$  exhibits  $Fe-O$  and  $O-O$  stretching vibrations with Fermi splitting (hereafter “/”) centered at 470 and 897  $cm^{-1}$ , respectively (Figure S3). Also observed are weaker bands at 513/532  $cm^{-1}$  that downshift to 500  $cm^{-1}$  with  $^{18}O_2$ , which we therefore assign to the asymmetric  $Fe-O$  stretch of the  $Fe_2O_2$  core. Addition of  $H^+$  to  $1a \cdot O_2$  only marginally affects its RR spectrum, with a small upshift in  $Fe-O$  and downshift in  $O-O$  vibrations (Figure S3, Table 1). These shifts in RR frequencies upon  $H^+$  addition may reflect subtle changes in  $Fe-O-O-Fe$  angles<sup>16</sup> but are too small to support the conclusion that a ( $\mu$ -1,2-peroxo)diiron(III) unit has been converted to a (hydroperoxo)diiron(III) species. The RR spectrum of  $2 \cdot O_2$  is practically identical to that of  $1a \cdot O_2$ , with symmetric and asymmetric  $Fe-O$  modes at 466/475 and 513/532  $cm^{-1}$ , respectively, and Fermi-

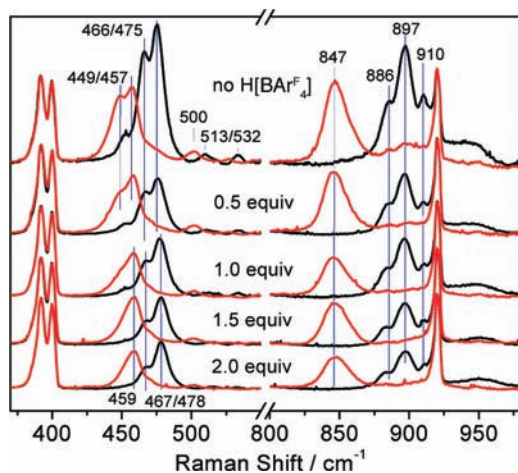


**Figure 2.** RR spectra of  $2 \cdot ^{16}O_2$  (black) and  $2 \cdot ^{18}O_2$  (red) after addition of 0, 0.5, 1.0, 1.5, and 2.0 equiv of  $H[Bar^F_4]$ . Each spectrum was normalized based on the solvent  $CH_3CN$  bands at 392, 400, and 920  $cm^{-1}$ .

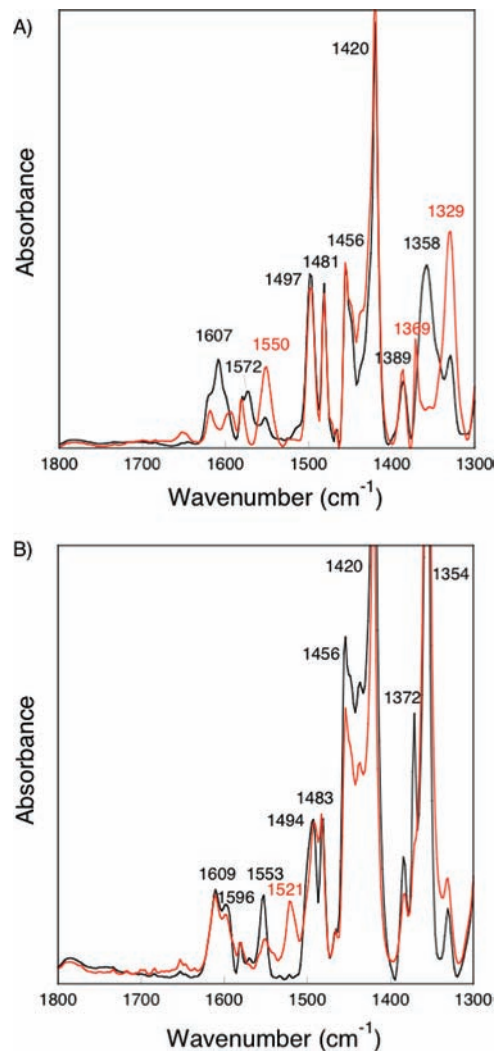


**Figure 3.** Solution FTIR spectra of  $1a \cdot O_2$  (black) and  $1b \cdot O_2$  (red) before (A, top) and after (B, bottom) the addition of 1.5 equiv of  $H[Bar^F_4]$ . The spectra were acquired in  $CH_2Cl_2$  at approximately  $-30$   $^{\circ}C$  with a diiron concentration of  $\sim 55$  mM. The intense peaks at 1354 and 1420  $cm^{-1}$  are due to the  $[Bar^F_4]^-$  anion and solvent, respectively.

coupled  $O-O$  stretches centered at 897  $cm^{-1}$  (Figure 2). Addition of up to 2.0 equiv of  $H[Bar^F_4]$  to generate  $[2 \cdot O_2]H^+$  primarily affects the symmetric  $Fe-O$  stretch, which upshifts only a few wavenumbers compared to the spectrum of  $2 \cdot O_2$  (Table 1). From the RR data and Mössbauer parameters for  $1a \cdot O_2$ ,  $[1a \cdot O_2]H^+$ ,  $2 \cdot O_2$ , and  $[2 \cdot O_2]H^+$ , we conclude that protonation does not lead to formation of a (hydroperoxo)diiron(III) species.

Since the benzimidazole, amino, and propoxy groups of *N*-EtHPTB are less accessible due to the multidentate nature of the ligand, we assign the carboxylate unit as the site of protonation. To test this hypothesis, we examined the carboxylate stretches of **1a** and **1b** and their peroxo complexes by FTIR spectroscopy. The assignment of frequencies in terms of coordination geometry are complicated by mixing of the  $COO^-$  symmetric stretch with the  $O-C-O$  bend and  $C-C$  stretch.<sup>17</sup> Nevertheless, if the asymmetric and symmetric  $COO^-$  stretches can be identified, the binding geometry of the carboxylate ligand can be derived from the difference in the two,  $\Delta\nu_{as-s}$ .<sup>18–20</sup> Specifically,  $\Delta\nu_{as-s}$  should be close to that of the free ionic form, 150  $cm^{-1}$  for  $PhCOO^-$ , for carboxylates bridging two metal ions, larger in unidentate coordination geometries, and smaller in

**Table 1.** UV–Vis, Mössbauer, RR, and FTIR Data for  $1\mathbf{a}\cdot\text{O}_2$ ,  $[1\mathbf{a}\cdot\text{O}_2]\text{H}^+$ ,  $2\cdot\text{O}_2$ , and  $[2\cdot\text{O}_2]\text{H}^+$ 

complex	$\lambda_{\text{max}}$ , nm ( $\epsilon$ , $\text{M}^{-1}\text{cm}^{-1}$ )	$\delta$ , mm/s	$\Delta E_{\text{O}}$ , mm/s	$\nu$ (Fe–O), $\text{cm}^{-1}$ ( $\Delta^{18}\text{O}$ )	$\nu$ (O–O), $\text{cm}^{-1}$ ( $\Delta^{18}\text{O}$ )	$\nu_{\text{as}}(\text{COO}^-)$ , $\text{cm}^{-1}$ ( $\Delta^{13}\text{C}$ )	$\nu_{\text{s}}(\text{COO}^-)$ , $\text{cm}^{-1}$ ( $\Delta^{13}\text{C}$ )
$1\mathbf{a}\cdot\text{O}_2$	590 (3100)	0.53(2)	0.71(2)	466/474 (–18)	897 (–50)	1607/1572 (>–22)	1358 (–29)
$[1\mathbf{a}\cdot\text{O}_2]\text{H}^+$	600 (2360)	0.53(2)	0.80(2)	467/478 (–20)	896 (–53)	1553 (–32)	–
$2\cdot\text{O}_2$	600 (3300)	0.53(2)	0.77(2)	466/475 (–18)	897 (–50)	–	–
$[2\cdot\text{O}_2]\text{H}^+$	610 (2700)	0.54(2)	0.84(2)	478 (–19)	897 (–50)	–	–

bidentate mononuclear complexes. As expected,  $1\mathbf{a}$  and  $1\mathbf{b}$  exhibit  $\Delta\nu_{\text{as-s}}$  values of 166 and 149  $\text{cm}^{-1}$ , respectively, consistent with  $\mu$ -1,3 bridging carboxylate groups (Figure S4B). In  $1\mathbf{a}\cdot\text{O}_2$ ,  $\nu_{\text{as}}$  and  $\nu_{\text{s}}$  are at 1572/1607 and 1358  $\text{cm}^{-1}$ , respectively, and, in  $1\mathbf{b}\cdot\text{O}_2$ , are at 1550 and 1329  $\text{cm}^{-1}$  (Figure 3A). Owing to multiple observed values of  $\nu_{\text{as}}$  and  $\nu_{\text{s}}$  for  $1\mathbf{a}\cdot\text{O}_2$  and  $1\mathbf{b}\cdot\text{O}_2$  we cannot unambiguously determine their carboxylate coordination geometries from  $\Delta\nu_{\text{as-s}}$  values.<sup>21</sup> Generation of  $[1\mathbf{a}\cdot\text{O}_2]\text{H}^+$  and  $[1\mathbf{b}\cdot\text{O}_2]\text{H}^+$  is associated with a downshift of the  $\nu_{\text{as}}$  modes by at least 20  $\text{cm}^{-1}$ , whereas  $\nu_{\text{s}}$  modes are not observed, possibly shifting below 1300  $\text{cm}^{-1}$  (Figure 3B). Most importantly, the FTIR spectra in both  $\text{CH}_2\text{Cl}_2$  and  $\text{CD}_3\text{CN}$  (Figure S5) show no evidence of free benzoic acid. With the use of the less basic carboxylate  $\text{C}_6\text{F}_5\text{CO}_2^-$ , present in  $2$ , protonation leads to free pentafluorobenzoic acid, but only in the coordinating solvent acetonitrile and not in  $\text{CH}_2\text{Cl}_2$  (Figure S6).

A comparison of the  $^1\text{H}$  NMR spectra of the benzoate and pentafluorobenzoate diiron complexes allows the phenyl ring protons of the former to be identified in  $1\mathbf{a}\cdot\text{O}_2$  as paramagnetically broadened peaks at 7.0, 8.7, and 11.4 ppm (Figure S7A). Upon addition of  $\text{H}[\text{BAr}^{\text{F}}_4]$ , these resonances shift to 7.5, 8.0, and 9.8 ppm (Figure S7C), in support of the protonation of the benzoate ligand. This conclusion is confirmed by analysis of the  $^{19}\text{F}$  NMR spectra of  $2\cdot\text{O}_2$  and  $[2\cdot\text{O}_2]\text{H}^+$ . The fluorine resonances of the pentafluorobenzoate ring in  $2\cdot\text{O}_2$  appear at –134.34, –154.44, and –159.02 ppm (Figure 4A) and shift to –111.30, –142.96, and –154.79 ppm upon addition of 3 equiv of  $\text{H}[\text{BAr}^{\text{F}}_4]$  (Figure 4B). These results demonstrate that the  $\text{C}_6\text{F}_5\text{CO}_2\text{H}$  ligand is bound to iron in dichloromethane. Once again, only in the coordinating solvent acetonitrile are resonances for free pentafluorobenzoic acid observed (Figure S8).

In conclusion, the spectroscopic evidence (Table 1) clearly indicates that the carboxylate is preferred over the peroxo ligand as the site of protonation in these (peroxo)diiron(III) model

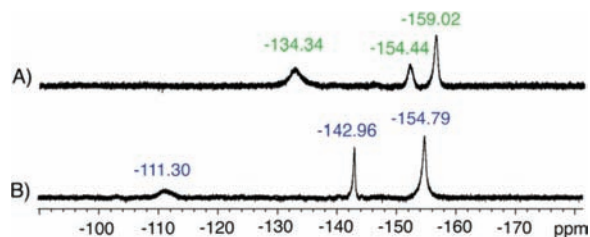


**Figure 4.**  $^{19}\text{F}$  NMR spectra (470 MHz,  $\text{CD}_2\text{Cl}_2$ ,  $-30\text{ }^\circ\text{C}$ ) of  $[2\cdot\text{O}_2](\text{OSO}_2\text{CF}_3)_2$  (A) and  $[2\cdot\text{O}_2](\text{OSO}_2\text{CF}_3)_2/\text{H}[\text{BAr}^{\text{F}}_4]$  (1:3) (B).

complexes, a possible structure for which is depicted in Scheme 1. Our results suggest that, during the  $\text{O}_2$  activation steps in the catalytic cycle of sMMO and related enzymes, protons might generate and/or transform the (peroxo)diiron(III) core by inducing a carboxylate shift,<sup>22,23</sup> possibly increasing the electrophilicity of the diiron unit and facilitating substrate access to the active site. Future work with synthetic analogues will address these important questions.

**Acknowledgment.** This work was supported by Grants GM032134 (S.J.L.) and GM74785 (P.M.-L.) from the National Institute of General Medical Sciences.

**Supporting Information Available:** Synthesis and characterization of diiron(II) complexes, experimental procedures, and spectroscopic data. This material is available free of charge via the Internet at <http://pubs.acs.org>.

## References

- Feig, A. L.; Lippard, S. J. *Chem. Rev.* **1994**, *94*, 759–805.
- Wallar, B. J.; Lipscomb, J. D. *Chem. Rev.* **1996**, *96*, 2625–2658.
- Vu, V. V.; Emerson, J. P.; Martinho, M.; Kim, Y. S.; Münck, E.; Park, M. H.; Que, L., Jr. *Proc. Natl. Acad. Sci. U.S.A.* **2009**, *106*, 14814–14819.
- Nordlund, P.; Reichard, P. *Annu. Rev. Biochem.* **2006**, *75*, 681–706.
- Fox, B. G.; Lyle, K. S.; Rogge, C. E. *Acc. Chem. Res.* **2004**, *37*, 421–429.
- Merkx, M.; Kopp, D. A.; Sazinsky, M. H.; Blazyk, J. L.; Müller, J.; Lippard, S. J. *Angew. Chem., Int. Ed.* **2001**, *40*, 2782–2807.
- Leahy, J. G.; Batchelor, P. J.; Morcomb, S. M. *FEMS Microbiol. Rev.* **2003**, *27*, 449–479.
- Liu, K. E.; Wang, D.; Huynh, B. H.; Edmondson, D. E.; Salifoglou, A.; Lippard, S. J. *J. Am. Chem. Soc.* **1994**, *116*, 7465–7466.
- Moënné-Loccoz, P.; Baldwin, J.; Ley, B. A.; Loehr, T. M.; Bollinger, J. M., Jr. *Biochemistry* **1998**, *37*, 14659–14663.
- Murray, L. J.; Naik, S. G.; Ortillo, D. O.; García-Serres, R.; Lee, J. K.; Huynh, B. H.; Lippard, S. J. *J. Am. Chem. Soc.* **2007**, *129*, 14500–14510.
- Lee, S.-K.; Lipscomb, J. D. *Biochemistry* **1999**, *38*, 4423–4432.
- Tinberg, C. E.; Lippard, S. J. *Biochemistry* **2009**, *48*, 12145–12158.
- Dong, Y.; Ménage, S.; Brennan, B. A.; Elgren, T. E.; Jang, H. G.; Pearce, L. L.; Que, L., Jr. *J. Am. Chem. Soc.* **1993**, *115*, 1851–1859.
- Dong, Y.; Yan, S.; Young, V. G., Jr.; Que, L., Jr. *Angew. Chem., Int. Ed. Engl.* **1996**, *35*, 618–620.
- Jensen, K. P.; Bell, C. B., III; Clay, M. D.; Solomon, E. I. *J. Am. Chem. Soc.* **2009**, *131*, 12155–12171.
- Brunold, T. C.; Tamura, N.; Kitajima, N.; Moro-oka, Y.; Solomon, E. I. *J. Am. Chem. Soc.* **1998**, *120*, 5674–5690.
- Nara, M.; Torii, H.; Tasumi, M. *J. Phys. Chem.* **1996**, *100*, 19812–19817.
- Deacon, G. B.; Phillips, R. J. *Coord. Chem. Rev.* **1980**, *33*, 227–250.
- Nakamoto, K. *Part B: Applications in Coordination, Organometallic, and Bioinorganic Chemistry*, 5th ed.; John Wiley & Sons, Inc.: New York, 1997.
- Costas, M.; Cady, C. W.; Kryatov, S. V.; Ray, M.; Ryan, M. J.; Rybak-Akimova, E. V.; Que, L., Jr. *Inorg. Chem.* **2003**, *42*, 7519–7530.
- Martínez, D.; Motevalli, M.; Watkinson, M. *Dalton. Trans.* **2010**, *39*, 446–455.
- Dunietz, B. D.; Beachy, M. D.; Cao, Y.; Whittington, D. A.; Lippard, S. J.; Friesner, R. A. *J. Am. Chem. Soc.* **2000**, *122*, 2828–2839.
- Rinaldo, D.; Philipp, D. M.; Lippard, S. J.; Friesner, R. A. *J. Am. Chem. Soc.* **2007**, *129*, 3135–3147.

JA909718F